Am J Nucl Med Mol Imaging 2019;9(1):1-11
www.ajnmmi.us /ISSN:2160-8407/ajnmmi0087540

Original Article

Tissue volume and activity mapping using total intensity projection of PET/CT images

Rozh H Al-Mashhadi[1,2,3], Jacob F Bentzon[1,3,5], Lars P Tolbod[4]

Departments of [1]Clinical Medicine, [2]Radiology, [3]Cardiology, [4]Nuclear Medicine and PET Center, Aarhus University Hospital, Aarhus, Denmark; [5]Centro Nacional de Investigaciones Cardiovasculares Carlos III, Madrid, Spain

Received October 29, 2018; Accepted December 3, 2018; Epub February 15, 2019; Published February 28, 2019

Abstract: Autoradiography using phosphor imaging screens is often used to characterize tissue distribution of positron emission tomography (PET) radiotracers. PET tracers emit positrons with limited penetration range, and valid quantitative autoradiography can therefore only be achieved in thin tissue slices. However, in some settings, quantitative tracer profiling in thick tissues is required. Our aim was to develop a reliable method for this purpose. In this paper, we present a method based on total intensity projections (TIPs) of PET and computed tomography (CT) images. We show theoretically and experimentally that tissue total activity and tissue volume maps can be derived from the TIPs of PET and CT images, respectively. We also show that these maps are free of signal displacement artifacts in the direction of projection. To demonstrate the utility of the approach, we obtain and compare TIP-based maps and autoradiography of ex-vivo atherosclerotic minipig aortas following in-vivo injection of ^{18}F-fluorodeoxyglucose. We show that autoradiography of the thick aortas yields distorted results due to positron range effects, whereas TIP-mapping is free from such bias. The TIP-based maps may, thus, provide a low-resolution alternative to autoradiography, when tracer accumulation profiling in thick tissues is required.

Keywords: Autoradiography, total intensity projection, activity map, volume map, signal displacement effects

Introduction

Accurate quantification of the accumulation profile of positron emission tomography (PET) radiotracers in tissues is pivotal for clarification of their specificity towards different tissue types and their utility in imaging of disease processes. Autoradiography is an important tool, commonly used for quantification of tissue distribution of novel and existing radiotracers. Often conducted using storage phosphor screens, autoradiography is generally considered the *gold standard* in nuclear medicine, providing high resolution visualization of tissue tracer distribution. However, for most tracer radioisotopes, the signal recorded by autoradiography reflects only tracer content in a thin layer at the surface of the tissues. This is because the particles emitted by many radioisotopes have only limited penetration power, i.e. only particles released from a thin layer at the tissue surface may reach the phosphor screens. This effect is most pronounced in the case of ^{3}H, a commonly used tracer isotope. ^{3}H decays by emission of electrons with a kinetic energy in the range 0-18.6 (mean 5.7) keV and only electrons emitted from a few μm thin layer at the surface of tissues are able to escape and reach the phosphor screens [1]. In the case of PET radioisotopes, e.g. the widely used ^{18}F, the primary emission is predominantly a positron that undergoes annihilation producing two high-energy photons at 511 keV. Due to their high energy, these photons are expected to pass through the thin (115 μm [1]) detection layer of the phosphor screens, without interaction. Prior to annihilation, the positrons emitted from ^{18}F have kinetic energies in the range of 0-635 (mean 252) keV, and those reaching the screens with a proper energy level, will interact leaving an imprint. Importantly, the penetration power of the ^{18}F positrons is limited, with half of the positrons expected to annihilate within approximately 200 μm in the tissue itself [2]. Thus, also in the case of ^{18}F and other positron emitters with similar emission energies, the

autoradiography signal will mainly reflect tracer distribution at the tissue surface with deeper tissues having increasingly less contribution.

Positron range constraints are a minor concern when autoradiography is conducted with thin histological slices of less than 100 μm. However, in certain experimental settings, information is required on tracer accumulation in large tissue specimens, and thin histological sectioning may be impractical or infeasible. In such cases, thick tissue segments up to several millimeters, or even whole organ specimens, have been used to acquire autoradiographic images of positron emitting tracers [3-8]. This approach, however, may not quantitively depict radiotracer distribution due to overlapping tissues and positron range effects. Furthermore, autoradiography provides a profile of total tissue activity projected on the screens, not tissue activity concentration. If the tissues are not sliced at uniform thickness [3-6, 8], the autoradiography signal may also reflect variability in tissue thickness which may additionally distort the signal profile.

Conducting ex-vivo PET scans may provide an alternative method for tracer profiling in thick (e.g. 1-5 mm) tissues. In contrast to autoradiography, PET provides a profile of the activity concentrations in the tissues. However, if tissue dimensions are less than 2-3 times scan resolution, incomplete signal recovery may be obtained obscuring the actual tracer profile [9]. The relatively low resolution of PET at approximately 6-8 mm [10] leads to signal displacement effects, also referred to as partial volume effects, distorting the activity concentrations in a volume-dependent manner [9].

As an alternative method for acquiring tracer profiles in thick tissues, we developed the total intensity projection (TIP) of PET and computed tomography (CT) images. In this paper, we present theoretical derivations showing that the TIP of PET (TIP_{PET}) and CT (TIP_{CT}) imaging volumes can be converted into tissue total activity and tissue thickness/volume maps, respectively. We also show theoretically that these maps are free of signal displacement artefacts in the direction of projection. We validate these theoretical predictions using PET/CT scans of phantoms with known thickness and tracer activity concentration. To demonstrate the utility of this approach, we examine the distribution of ^{18}F-fludeoxyglucose (FDG) in thick atherosclerotic aortas and show that the TIP approach provides more accurate data compared with autoradiography. The approach may, thus, be used as a low-resolution alternative to autoradiography in cases where quantitative tracer profiling in thick tissues is required.

Methods

Preparation of PET/CT phantoms

A solution of 3% agarose (Sigma-Aldrich, Denmark) in demineralized water was mixed with FDG resulting in an activity concentration of 113 kBq/ml. The mixture was left to harden for app. 1½ hours in a cylindrical container with an inner diameter of 65 mm. Subsequently 0.5, 1, 2, 4, 7 and 10 mm thick discs were sliced out, placed between two 10 mm thick methylmethacrylate polymer plates (Plexiglas, Evonik, Germany) and PET/CT scanned. The methacrylate plates were used to provide an annihilation medium for the emitted positrons. Four discs of each thickness were scanned, i.e. 24 discs in total. One agarose block of 40 mm thickness was included in all scans and used as the reference to measure the true activity concentration, i.e. activity concentration that is not affected by partial volume effects. The activity concentration in the reference block was determined as the mean value of a volume in the middle of the block at least 1.5 cm away from the edges. Due to radioactive decay, the activity concentrations measured in the reference block were 25-45 kBq/ml at times of the scans.

Animals used for ex-vivo PET/CT scans and autoradiography

Ex-vivo *en-face* autoradiography and PET/CT scans were conducted of 4 aortas from atherosclerotic Yucatan minipigs. The animals were part of a concurrent study, and details on the experimental procedures were reported previously [11, 12]. Briefly, 3 D374Y-PCSK9 and 1 wildtype minipigs were fed a high fat high cholesterol diet for almost 1 year. The animals were injected with 415 (± 11, standard deviation, SD) MBq FDG and were euthanized after a circulation time of 118 (± 13, SD) minutes. The aortas were quickly extracted and opened along the minor curvature. Blood was wiped off and the perivascular tissues carefully removed,

and the aortas were *en-face* ex-vivo PET/CT scanned at 181 (± 28, SD) minutes following the in-vivo FDG injection. Subsequently, the aortas were placed *en-face* and the luminal surface was pressed tightly onto autoradiography phosphor imaging screens (BAS-IP, TR20-25E, GE Healthcare, UK) that were wrapped in shrink-wrap (app. 10 μm in thickness) for protection from moisture. The screens were stored at room temperature for an exposure period of 2 hours and subsequently scanned with a Fuji Analyzer BAS-5000 (Fuji, Japan). No saturation of the signal on the phosphor screens occurred (The software of the Fuji Analyzer BAS-5000 automatically marked regions with saturation). All animal procedures were approved by the Danish Animal Experiments Inspectorate.

PET/CT scans of phantoms and minipig aortas

A 64-slice PET/CT scanner (Discovery 690; GE Healthcare) was used to conduct scans of phantoms and ex-vivo scans of pig aortas using 1 and 2 PET bed positions, respectively, each with a duration of 10 minutes. PET images were reconstructed using a 3D OSEM algorithm with time-of-flight correction and resolution recovery. Images were reconstructed at a resolution of 1.82×1.82×3.27 mm (VuePoint FX SharpIR, 3 iterations, 24 subsets, 4 mm 2D Gaussian post-filter in transaxial plane and a 3-point convolution post-filter [1 6 1] in the axial direction). An initial CT scan was used for localization and attenuation correction (120 kV, 240 mA, 1.25-mm slice thickness).

Analyses of TIP-derived volume and activity maps

Total intensity projections of CT and PET imaging volumes were generated by calculating the sum of voxel values for all voxel columns perpendicular to the direction of projection. Subsequently, the TIP_{CT} was converted into tissue thickness and tissue volume maps through multiplication of each pixel in the TIP plane by CT voxel thickness and voxel volume, respectively. The TIP_{PET} was converted into a tissue total activity map through multiplication of the TIP values by the PET voxel volume. To account for reconstruction matrix size, the total activity map can be presented as activity per area through division by area of each pixel in the projected plane. Calculations of the TIP-derived maps are detailed in the **Appendix**.

Of the 24 agarose phantom discs, 75 small pieces were cut out and micrograph images were obtained to measure their true thickness. The thickness/volume maps were validated by comparing the TIP_{CT}-derived thickness with the true thickness measured on the micrographs.

For validation of the total activity maps derived from TIP_{PET}, the maps were converted to activity concentration maps through pixel-wise division by the volume maps. The activity concentration maps of the 0.5-10 mm thick phantoms were then compared with the true activity concentration that was measured directly on the PET images in the 40-mm reference block. Recovery fractions were calculated through division of the TIP-derived activity concentrations by the true activity concentration.

Determination of signal generation mechanism for positron emitters on storage phosphor screens

Two solutions of FDG were prepared with activity concentrations of 500 kBq/ml and 50 kBq/ml, respectively. From each solution, 5 μl was applied on 5 pieces of paper and were left to dry for few minutes. Activities from the 10 radioactive sources were recorded on phosphor imaging screens. For each of the two activity levels, one activity source was opposed directly on the phosphor screens, while the other sources were separated by a radiation barrier consisting of an increasing number of layers of plastic (low density polyethylene). Each layer of the plastic material was 70 μm in thickness. Imaging screens were stored at room temperature for an exposure period of 3 hours. To analyze the acquired data, digital autoradiographic images were converted to photo-stimulated luminescence (PSL) units. The average background activity per area was determined by measuring the average signal on a region of the phosphor screen far away from opposed activity sources. The total activity from each source was measured by drawing a region of interest (ROI) that covered a large area containing the stored FDG signal but also surrounding area containing only background. The total background signal (calculated as the measured average background multiplied by ROI area) was then subtracted to yield the net total activity from each activity source. The profile of signal attenuation as a function of plastic barrier thickness was fitted to a double exponential equation, as reported previously [13].

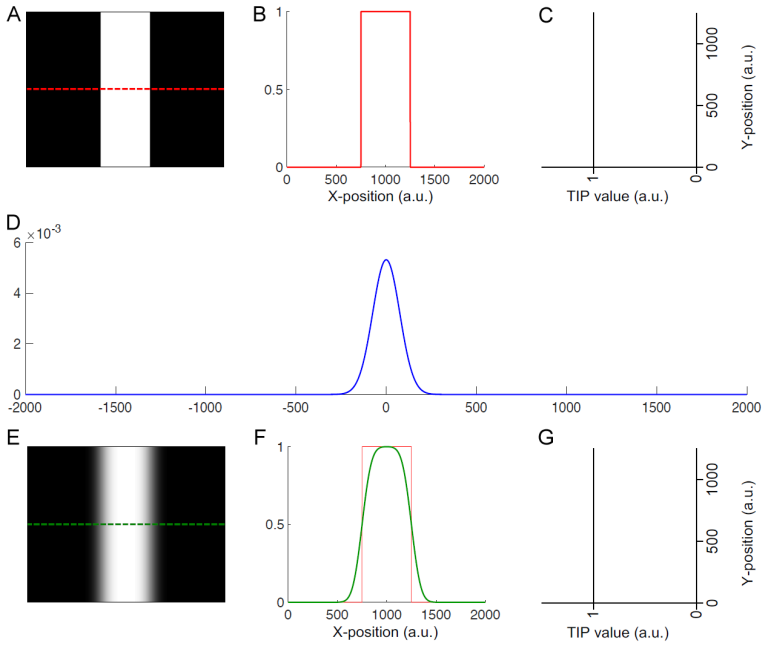

Figure 1. Simulation of the effect of convolution on the total intensity projection (TIP). (A, B) Cross-section of a sharply bordered structure (A) and its signal profile (B) with nominal signal magnitude set to 1. (C) The TIP of the signal calculated for projection along the x-direction (horizontal). (D) Hypothetical Gaussian point spread function with area under the curve equal to 1. (E) Simulation of the blurred signal of (A) as it would appear on a CT or PET scan. The blurring is the result of convolution of (A) by (D). (F) Profile of the blurred signal (green curve). (G) The TIP of the signal seen in (F). Convolution spreads the signal but does not alter the total signal magnitude, i.e. the area under the curve (AUC). The TIP is equal to the AUC and, thus, recovers the full original signal magnitude (G). a.u.: arbitrary units.

Data availability

The datasets generated during and analyzed during the current study are available from the corresponding author on reasonable request.

Results

Tissue volume and total activity maps based on total intensity projection of CT and PET imaging data

We aimed to develop a method for quantitative assessment of radiotracer distribution in thick tissues by total intensity projections of ex-vivo PET/CT scans. We defined TIP as the sum of voxel values in columns perpendicular to the plane of projection. The TIP_{CT} can be multiplied by voxel thickness to create a tissue thickness map or by voxel volume to create a tissue volume map. The TIP_{PET} can be multiplied by voxel volume to create tissue total activity map. In addition, the total activity map may be divided by the volume map to generate an activity concentration map. The theoretical derivations describing how the TIPs are converted to maps are presented in the **Appendix**.

TIP-based maps yield full signal recovery in the direction of projection

Imaging systems suffer often from signal displacement artifacts that are the result of two distinct aspects of the acquisition and reconstruction operations, namely 1) blurring or convolution by the point spread function (PSF) of the imaging system and 2) a limited spatial sampling frequency i.e. relatively large reconstruction voxels. Both effects lead to displacement of signal causing incomplete signal recovery [9], although the overall magnitude of the total signal is preserved. The TIP operation accumulates the signal along the direction of projection, reproducing the original full signal, thus effectively counteracting the effect of blurring, as explained in **Figure 1**. Furthermore, multiplying the TIP of the signal by voxel dimensions to yield tissue thickness/volume or total activity, corrects for the second effect relating to the spatial sampling, as illustrated in **Figure 2**. Thus, theoretically, all TIP-derived maps are free of signal displacement artifacts along the direction of projection.

To validate these theoretical predictions, a series of phantom scans were conducted. First, thickness maps derived from TIP_{CT} images were compared with actual thickness of agarose phantoms. Direct proportionality was observed between TIP_{CT}-derived thickness and true thickness of the agarose phantoms, demonstrating that TIP_{CT}-derived thickness maps, and equivalently volume maps, were relieved from signal displacement artifacts, perfectly reproducing the target thickness (**Figure 3A**). Second, TIP_{PET}-derived activity maps were converted to activity concentration maps through division by TIP_{CT}-derived volume maps. The activity concentra-

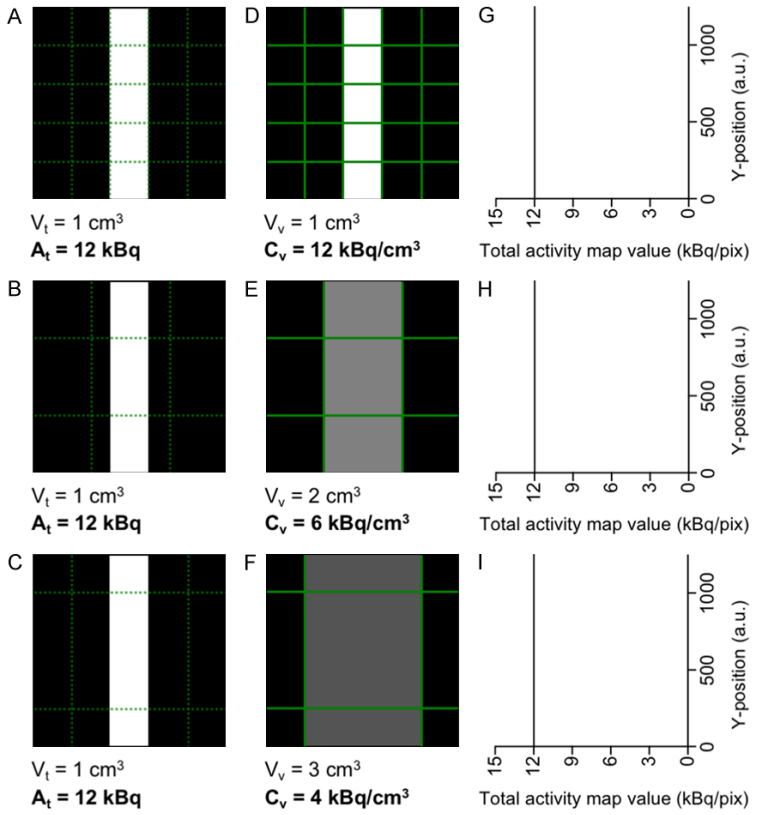

Figure 2. Simulation of the effect of voxel volume on TIP-derived volume-maps. (A-C) Cross-sections of a sharply bordered target structure. The grid represents the reconstruction matrix. V_t: target structure volume within each voxel. A_t: total activity of target structure in each voxel. (D-F) Illustrations of the sampled images of (A-C). A mismatch between tissue and voxel dimensions (E, F) leads to altered representation of target activity concentration on the reconstructed images. V_v: voxel volume. C_v: activity concentration in target-containing voxels. (G-I) TIP-derived activity map values calculated based on (D-F). The direction of projection is horizontal (x-direction). Calculation of the activity maps takes both voxel signal concentration (C_v) and voxel volume into account enabling full recovery of tissue total activity A_t (A-C). While the *activity concentration* values measured directly in the voxels suffer from incomplete signal recovery, the mapping approach yields full recovery of *total activity* (D-F). The activity maps are, thus, unaffected by signal displacement artifacts caused by large voxel volumes.

tion maps provided virtually full signal recovery with recovery fractions close to 100% (**Figure 3B**). By contrast, when the activity concentrations were measured directly on the PET images, partial volume artifacts [9] severely affected the recovery fractions that were as low as 6% for the 0.5 mm thick phantoms and reaching only 64% for the 10 mm phantoms (data not shown). Thus, although PET, and to lesser extent CT, are low-resolution imaging techniques that suffer from signal displacement effects, these artifacts were corrected and rendered negligible in the direction of projection by the TIP-based analyses.

Autoradiography and TIP analyses of atherosclerotic arteries

To demonstrate the utility of TIP-based tracer mapping, we conducted ex-vivo PET scans and autoradiography of atherosclerotic minipig aortas, following in-vivo injection of FDG. FDG is reported to accumulate predominantly in metabolically active macrophages in atherosclerotic plaques [14, 15], although other arterial cell types, including vascular smooth muscle cells, have also been implicated in FDG accumulation [16]. The prevailing view is that FDG accumulates preferentially in plaques compared with normal arterial wall in both humans and animals [17].

We found that *en face* autoradiography of atherosclerotic aortas yielded highly variable and inconsistent results. Some atherosclerotic lesions exhibited, as expected, high signal compared with surrounding normal vessel wall, while other lesions displayed equal or, even lower signal compared with non-lesioned sites. An example of the unexpected lower signal in plaques compared with normal wall is provided in **Figure 4B**. By contrast, the TIP-derived total activity map showed consistently higher total activity in atherosclerotic lesions compared with surrounding normal tissues (**Figure 4C**), consistent with the expected increase in FDG accumulation at lesioned sites [17]. A slice through the artery from the original PET image is also shown in **Figure 4D** to illustrate differences between the original PET slices and the TIP-derived volume map.

Autoradiography signal generation mechanism

To clarify the inconsistent and variable results obtained with autoradiography, we aimed to

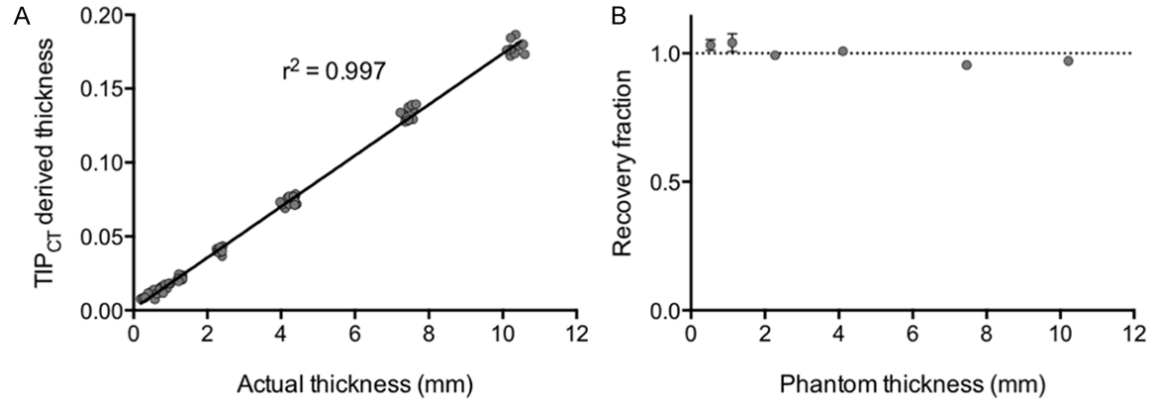

Figure 3. Validation of TIP_{CT}-derived thickness and TIP_{PET}-derived total activity measurements. (A) Agarose phantoms with variable thickness (0.5 mm-10 mm) were PET/CT scanned. Direct proportionality is seen between TIP_{CT}-derived optical thickness and actual thickness of agarose phantoms, measured on micrograph images, demonstrating that TIP_{CT}-derived thickness mapping is unaffected by signal displacement artifacts. (B) TIP_{PET}-derived total activity maps were divided by TIP_{CT}-derived volume maps to yield activity concentration maps. The phantoms contained a known amount of FDG. Virtually complete signal recovery for phantoms of different thicknesses is seen. A full signal recovery implies no or negligible effect of signal displacement artifacts on TIP_{PET}-derived total activity and activity concentration maps. Data are mean ± standard error of the mean.

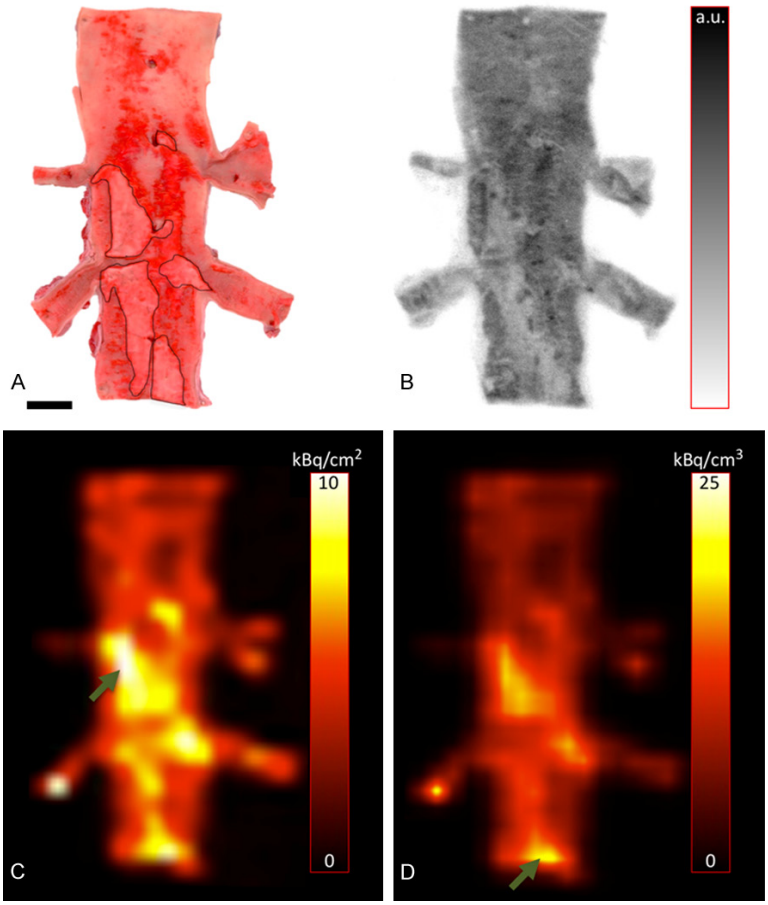

Figure 4. Example of an atherosclerotic aorta from an FDG-injected minipig. (A) A segment of the abdominal aorta is opened and presented *en face* following staining with Sudan IV that stains fatty steaks red. Raised plaque areas are delineated for demonstration. Scale bar is 1 cm. (B) Autoradiography of the specimen shown in (A). Note how the raised atherosclerotic lesions display, unexpectedly, lower signal intensities compared with neighboring artery wall regions. (C) TIP_{PET}-derived total activity map of the same artery segment. The raised atherosclerotic lesions display, as expected, higher signal intensities compared with neighboring artery wall regions. In-plane resolution of the activity map (C) is lower than the resolution of autoradiography (B), but sufficient to discern the atherosclerotic plaques. Note that autoradiography is also a projection of total activity, making (B) and (C) directly comparable. (D) A regular PET slice (without projection) of the same artery. To enable direct visual comparison between (C) and (D) the dynamic range of the color-coding scale was set to the maximum pixel value in each image, respectively. Note the quantitative differences in signal between (C) and (D), e.g. the area of highest signal intensity (arrows).

investigate the contribution of positrons and long-range gamma-rays to the autoradiography signal.

We exposed the phosphor screens to FDG sources that were covered by plastic shielding of variable thickness.

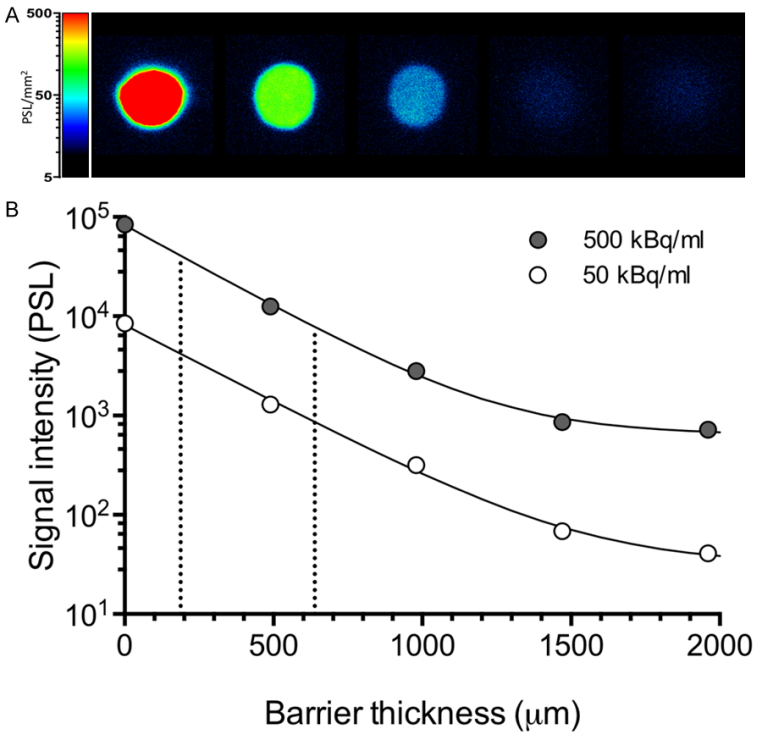

Figure 5. Mechanism of signal generation by positron emitters on phosphor imaging screens. (A) An autoradiography screen exposed to 5 sources of FDG with equal concentration (500 kBq/ml). The left-most source was placed directly on the screen, while the other sources were covered by plastic barriers of increasing thickness. The signal intensities are color-coded according to the displayed logarithmic scale. (B) Signal intensity as a function of barrier thickness. Data are presented for two concentrations of FDG as indicated. The left and right dotted lines indicate barrier thickness at which 50% and 90% of the signal is attenuated, respectively. Best-fit curves using double-exponential fitting are shown ($r^2 > 0.99$ for both curves). PSL: photostimulated luminescence.

Relatively thin barriers of plastic were able to shield a substantial portion of the emitted radiation (**Figure 5**). The barrier thickness leading to 50% signal attenuation, known as the half value layer (HVL) for the 500 kBq and 50 kBq sources was 183 μm and 194 μm, respectively. One mm of the plastic material attenuated app. 97% of the total signal for both sources. Annihilation of positrons results in generation of high energy photons (511 keV) that would readily penetrate 1 mm of plastic with negligible attenuation. The almost complete signal attenuation provided by 1 mm of plastic is, therefore, incompatible with photons playing a notable role in signal generation on phosphor imaging autoradiography screens.

These results, thus, confirmed that autoradiography signal obtained from the aortas was generated by positrons with limited penetration power, so the signal reflected tracer distribution primarily at the surface of tissues with deeper layers having less importance. The total thickness of the aortic wall was between 0.5 mm and 2.5 mm, while the penetration of positrons is orders of magnitude shorter [2]. Thus, it appeared that the location of the tracer-avid cells within the artery wall determined the proportion of the emitted positrons that reached the imaging screens making the autoradiography signal unrepresentative of the tracer uptake in the whole artery wall. By contrast, the TIP-derived activity maps did not suffer from the signal depth problem and provided expected and consistent results (**Figure 4**).

Discussion

En face autoradiography of opened vessels using positron emitters has been widely applied to study the distribution of FDG and other radiotracers across atherosclerotic arteries in mice, rabbits and pigs [3-6]. Autoradiography of thick tissue specimens has also been used to delineate FDG uptake in other types of tissues, including muscle tissues, adipose tissues and brain tissues [7, 8]. Such studies are performed to describe tracer localization with higher fidelity than can be achieved in vivo, and are performed under the implicit assumption that imaging screens are able to pick up signal from the entire, or at least a substantial fraction of the tissue specimen. However, this assumption is generally not met, except for very thin tissues, because of the limited penetration depth of the positrons that generate signal on the phosphor imaging screen.

Water constitutes a large proportion (60%-70%) of biological soft tissues. Monte Carlo simulations have previously been conducted to characterize the annihilation profile of positrons emitted from an ^{18}F point source in water [2],

and a calculation that we conducted based on these results yielded an HVL of app. 200 μm. As we showed on **Figure 5**, only the positrons, and not photons, participated in generation of the autoradiography signal. This means that signal recorded on autoradiography phosphor screens represents predominantly tracer distribution at the surface of the tissue, with deeper tissues having increasingly less contribution, due to annihilation of positrons traveling through the tissue itself. If the distribution of the tracer at the surface is not representative of tracer accumulation in deeper parts of the tissue, autoradiography may, thus, produce misleading signal. We show this to be the case for atherosclerotic minipig aortas, where normal whole-tissue autoradiography was not able to produce a consistent and reliable picture of tracer accumulation across the arterial wall and atherosclerotic plaques.

The TIP-based approach presented here is an alternative to autoradiography, where total activity maps can be constructed using TIP of the PET images. It does not have the resolution of autoradiography, but it is able to describe the full signal in the tissue of interest without signal displacement artifacts in the direction of the projection. When structures of interest are relatively large, e.g. atherosclerotic aortas, and the direction of projection is chosen carefully, e.g. perpendicular to the surface of opened vessels, this can provide clear description of differences in tracer uptake across tissue subcomponents, e.g. in atherosclerotic lesions compared to normal vessel wall. The approach is likely to be equally useful with other types of whole or sliced tissues.

The same principle, applied to CT images, renders accurate maps of tissue volume. Also this method is applicable to any type of tissue with approximately homogenous attenuation coefficients; a requirement fulfilled by most soft tissues. Having TIP_{CT}-derived volume maps and TIP_{PET}-derived activity maps, activity concentration maps with full signal recovery can be created. The original PET images (**Figure 4**) may be considered as activity concentration *weighted* images, because signal displacement artifacts cause the acquired signal to reflect, not only true activity concentration, but also size of the imaged structures [9]. By contrast, our projected maps do not suffer from such artifacts in the direction of projection. These maps can, thus, collectively provide information on tracer accumulation in thick tissues that is unattainable otherwise. The in-plane resolution, i.e. resolution of the resulting projection will be equal to the resolution of the original PET image.

In conclusion, we have shown that the limited positron range renders phosphor screen autoradiography unsuitable for quantitative investigation of positron-emitting PET tracer distribution profiles in thick tissue sections. For such applications, we have presented TIP-based analyses that provide projected maps of volume, activity and concentration. We have shown that these maps are free of signal displacement artifacts in the direction of projection. The maps may be used as an alternative to autoradiography in cases where tracer accumulation profile in thick tissue specimens in required. We illustrate the method using a full-size PET/CT scanner, but the method can also be utilized in a micro-PET scanner, whereby higher spatial resolution may be obtained.

Acknowledgements

The Danish Heart Foundation. Aarhus University IDEAS fund.

Disclosure of conflict of interest

None.

Authors' contribution

RHA conceived and developed the concept of TIP-derived mapping of CT and PET images. RHA, LPT and JFB conducted ex-vivo scans of aortas. RHA and JFB conducted the autoradiography experiments. RHA and LPT conducted scans of phantoms. RHA wrote the software to generate the TIP-derived maps and conducted all data analyses. All authors critically revised and approved the paper.

Address correspondence to: Rozh H Al-Mashhadi, Departments of Clinical Medicine, Radiology, Cardiology, Aarhus University Hospital, Palle Juul-Jensens Boulevard 99,8200, Aarhus, Denmark. E-mail: rham@clin.au.dk

References

[1] Ohuchi H, Hatano Y. Tritium measurement using aphoto-stimulable phosphor BaFBr(I): Eu^{2+} plate. Proc Radiochim Acta 2011; 1: 49-53.

[2] Levin CS, Hoffman EJ. Calculation of positron range and its effect on the fundamental limit of positron emission tomography system spatial resolution. Phys Med Biol 1999; 44: 781-99.
[3] Tahara N, Mukherjee J, de Haas HJ, Petrov AD, Tawakol A, Haider N, Tahara A, Constantinescu CC, Zhou J, Boersma HH, Imaizumi T, Nakano M, Finn A, Fayad Z, Virmani R, Fuster V, Bosca L, Narula J. 2-deoxy-2-[18F]fluoro-d-mannose positron emission tomography imaging in atherosclerosis. Nat Med 2014; 20: 215-9.
[4] Pérez-Medina C, Binderup T, Lobatto ME, Tang J, Calcagno C, Giesen L, Wessel CH, Witjes J, Ishino S, Baxter S, Zhao Y, Ramachandran S, Eldib M, Sánchez-Gaytán BL, Robson PM, Bini J, Granada JF, Fish KM, Stroes ES, Duivenvoorden R, Tsimikas S, Lewis JS, Reiner T, Fuster V, Kjær A, Fisher EA, Fayad ZA, Mulder WJ. In vivo PET imaging of HDL in multiple atherosclerosis models. JACC Cardiovasc Imaging 2016; 9: 950-61.
[5] Matter CM, Wyss MT, Meier P, Späth N, von Lukowicz T, Lohmann C, Weber B, Ramirez de Molina A, Lacal JC, Ametamey SM, von Schulthess GK, Lüscher TF, Kaufmann PA, Buck A. 18F-choline images murine atherosclerotic plaques ex vivo. Arterioscler Thromb Vasc Biol 2006; 26: 584-9.
[6] Zhao Y, Kuge Y, Zhao S, Morita K, Inubushi M, Strauss HW, Blankenberg FG, Tamaki N. Comparison of 99mTc-annexin A5 with 18F-FDG for the detection of atherosclerosis in ApoE-/- mice. Eur J Nucl Med Mol Imaging 2007; 34: 1747-55.
[7] Putzu A, Valtorta S, Di Grigoli G, Haenggi M, Belloli S, Malgaroli A, et al. Regional differences in cerebral glucose metabolism after cardiac arrest and resuscitation in rats using [^{18}F] FDG positron emission tomography and autoradiography. neurocrit care. Springer US; 2017; 127: e6-9.
[8] Ishino S, Sugita T, Kondo Y, Okai M, Tsuchimori K, Watanabe M, Mori I, Hosoya M, Horiguchi T, Kamiguchi H. Glucose uptake of the muscle and adipose tissues in diabetes and obesity disease models: evaluation of insulin and β3-adrenergic receptor agonist effects by ^{18}F-FDG. Ann Nucl Med 2017; 31: 413-423.
[9] Soret M, Bacharach SL, Buvat I. Partial-volume effect in PET tumor imaging. J Nucl Med 2007; 48: 932-45.
[10] Ikari Y, Akamatsu G, Nishio T, Ishii K, Ito K, Iwatsubo T, Senda M. Phantom criteria for qualification of brain FDG and amyloid PET across different cameras. EJNMMI Phys 2016; 3: 23.
[11] Al-Mashhadi RH, Sørensen CB, Kragh PM, Christoffersen C, Mortensen MB, Tolbod LP, Thim T, Du Y, Li J, Liu Y, Moldt B, Schmidt M, Vajta G, Larsen T, Purup S, Bolund L, Nielsen LB, Callesen H, Falk E, Mikkelsen JG, Bentzon JF. Familial hypercholesterolemia and atherosclerosis in cloned minipigs created by DNA transposition of a human PCSK9 gain-of-function mutant. Sci Transl Med 2013; 5: 166ra1.
[12] Al-Mashhadi RH, Bjørklund MM, Mortensen MB, Christoffersen C, Larsen T, Falk E, Bentzon JF. Diabetes with poor glycaemic control does not promote atherosclerosis in genetically modified hypercholesterolaemic minipigs. Diabetologia 2015; 58: 1926-1936.
[13] Derenzo SE. Mathematical removal of positron range blurring in high resolution tomography. IEEE Trans Nucl Sci 1986; 33: 565-9.
[14] Tawakol A, Migrino RQ, Bashian GG, Bedri S, Vermylen D, Cury RC, Yates D, LaMuraglia GM, Furie K, Houser S, Gewirtz H, Muller JE, Brady TJ, Fischman AJ. In vivo 18F-fluorodeoxyglucose positron emission tomography imaging provides a noninvasive measure of carotid plaque inflammation in patients. J Am Coll Cardiol 2006; 48: 1818-24.
[15] Menezes LJ, Kotze CW, Agu O, Richards T, Brookes J, Goh VJ, Rodriguez-Justo M, Endozo R, Harvey R, Yusuf SW, Ell PJ, Groves AM. Investigating vulnerable atheroma using combined ^{18}F-FDG PET/CT angiography of carotid plaque with immunohistochemical validation. J Nucl Med 2011; 52: 1698-703.
[16] Folco EJ, Sheikine Y, Rocha VZ, Christen T, Shvartz E, Sukhova GK, Di Carli MF, Libby P. Hypoxia but not inflammation augments glucose uptake in human macrophages: Implications for imaging atherosclerosis with 18fluorine-labeled 2-deoxy-D-glucose positron emission tomography. J Am Coll Cardiol 2011; 58: 603-14.
[17] Sheikine Y, Akram K. FDG-PET imaging of atherosclerosis: do we know what we see? Atherosclerosis 2010; 211: 371-80.

Appendix

Total intensity projection

Total intensity projection (TIP) was defined as the cumulative intensity of all voxels in a column perpendicular to plane of projection:

Eqn. 1: $TIP = \sum_{i=1}^{n} v_i$

- $v_{1..n}$ intensity in voxels 1..n

PET scans

The TIP of a PET imaging volume (TIP_{PET}, Bq/cm^3) is the sum of activity concentrations in all voxels in a column perpendicular to plane of projection:

Eqn. 2: $TIP_{PET} = \sum_{i=1}^{n} C_i$

- $C_{1..n}$ the activity concentration in voxels 1..n (Bq/cm^3)

A tissue *activity* map (Bq) can be constructed through multiplication of TIP_{PET} by voxel volume. On *exvivo* scans of biological tissues, only tissue voxels contribute to the signal within each column of voxels and thus column total activity equals tissue total activity.

CT scans

To calculate the TIP of a CT imaging volume (TIP_{CT}), the CT voxel values must be first converted from CT numbers to attenuation coefficients in accordance to the Hounsfield unit scale linear transformation. Subsequently, the TIP_{CT} can be calculated as the sum of attenuation coefficients in all voxels in a column perpendicular to plane of projection:

Eqn. 3: $TIP_{CT} = \sum_{i=1}^{n} u_i$

- $\mu_{1..n}$ attenuation coefficients in voxels 1..n (cm^{-1})

The TIP_{CT} in each column of voxels, as defined in Eqn. 3, is theoretically proportional to the thickness of the imaged object in that column, when the object has uniform attenuation (see explanation in next section). However, to correct for the possible use of different voxel dimensions in different scans, the TIP_{CT} must be multiplied by voxel height to make the measurements consistent across scans. Similarly, the TIP_{CT} in a column is proportional to volume of imaged object in that column, but needs to be multiplied by voxel volume to be consistent across scans. Multiplication of TIP_{CT} by voxel dimensions to yield a measure of thickness/volume derives naturally from Beer-Lambert's law, as explained in the next section.

The relationship between TIP_{CT} and the Beer-Lambert's law

The Beer-Lambert's law describes the attenuation of gamma rays through an object of n layers:

Eqn. 4: $I = I_o \cdot e^{-\sum_i^n u_i d_i}$

- I_0: the intensity of the incoming radiation; *I:* the intensity of outgoing attenuated ray; $\mu_{1..n}$: the attenuation coefficient in layers 1..n; $d_{1..n}$: the distance the radiation must travel through layers 1..n, i.e. layer thickness (cm).

In a CT scan, all slices (layers) parallel to the plane of projection have equal thickness, *d*:

Eqn. 5: $I = I_o \cdot e^{-d\sum_{i=1}^{n} u_i} = I_o \cdot e^{-d \cdot TIP_{CT}}$

Note that TIP_{CT} multiplied by slice thickness (voxel height), *d*, is simply the total *optical thickness,* τ (dimensionless):

Eqn. 6: $\tau = d \cdot \sum_{i=1}^{n} u_i = d \cdot TIP_{CT}$

If the imaged object is homogenous with uniform attenuation, μ, then the optical thickness will be proportional to the actual thickness, *t*, of the object:

Eqn. 7: $\tau = d \cdot n \cdot \mu = t \cdot \mu$

Similar considerations apply to object volume calculations, but the TIP_{CT} must be multiplied by voxel volume rather than voxel height.

Non-uniform x-ray attenuation

If the imaged object consists of several components with different x-ray attenuations, each column of voxels in the imaging volume may be split into multiple sets, each containing a homogenous component of the imaged object. For each component, a *partial* optical thickness may be calculated in concordance with Eqn. 7. This partial optical thickness will be proportional with the actual thickness of that component (Eqn. 7). The total optical thickness of the entire object becomes:

Eqn. 8: $t = t_{c1} \cdot \mu_{c1} + t_{c2} \cdot \mu_{c2} + \ldots t_{cn} \cdot \mu_{cn}$

● $t_{c1..cn}$: thickness of object components 1..n in a column along the direction of projection; $\mu_{c1..cn}$: attenuation coefficients of object components 1..n.

To obtain the attenuation coefficients for each component, multivariable regression analysis based on Eqn. 8 can be conducted, incorporating τ (recorded on CT images) against actual tissue component thickness (measured directly e.g. on micrographs).